ChemComm

COMMUNICATION

View Article Online
View Journal | View Issue

Cite this: *Chem. Commun.*, 2022, 58, 13373

Received 16th October 2022,
Accepted 7th November 2022

DOI: 10.1039/d2cc05631c

rsc.li/chemcomm

Asymmetric chlorination of A_2–A_1–D–A_1–A_2 type non-fullerene acceptors for high-voltage organic photovoltaics†

Peiqing Cong,‡[ab] Xianda Li,‡[ac] Ailing Tang,*[ab] Jiang Wu,[ac] Jianhua Chen,[d] Lie Chen[e] and Erjun Zhou*[ab]

Herein, we synthesized an asymmetric A_2–A_1–D–A_1–A_2 type small molecule nonfullerene acceptor (NFA), HCl-BTA3, by chlorination on one side of A_1. The synergistic effect of the asymmetric structure and chlorination endows HCl-BTA3 with a large dipole moment, close molecular packing, and high-efficiency charge transfer and transport. After being blended with a carboxylate-based polymer donor, TTC-Cl, HCl-BTA3 achieved a high open-circuit voltage (V_{OC}) of 1.20 V and a satisfactory power conversion efficiency (PCE) of 11.2%, which are among the highest values for high-voltage carboxylate-based polymers.

As one of the renewable energy technologies, organic photovoltaics (OPVs) have received widespread attention due to their low cost, lightweight, and excellent solution-processability. Photovoltaic material design, an indispensable part of OPV development, continues to drive power conversion efficiency (PCE) to a higher value.[1] Within a few years, non-fullerene acceptors (NFAs) have gradually replaced fullerenes as the primary acceptor material with the advantages of tunable energy levels, strong absorption, and ordered π–π stacking. As a result, the PCEs of single junction OPVs based on polymer donors and NFAs have surpassed 19%,[2–5] showing excellent commercial potential.

The dominant small molecule NFAs mainly include three categories: low bandgap (LBG) A–DA′D–A type, middle bandgap (MBG) A–D–A type, and wide bandgap (WBG) A_2–A_1–D–A_1–A_2 type. Due to the multiple modifiable active sites, numerous symmetric molecular modification strategies have been developed, including ring extension, halogenation, alkyl substitution, *etc.*, aiming to adjust absorption, energy levels, and molecular stacking, thus improving photovoltaic performance. On the other hand, the asymmetric design also attracts much attention because it can generate some unique properties. For example, it will induce a large dipole moment in the target molecules, reducing the exciton binding energy and increasing the intramolecular charge transfer ability.[6,7] In addition, the increased dipole moment will enhance the intermolecular interaction, improving the molecular packing and order. The asymmetric design has been successfully applied to the central cores, side chains, and terminals in the A–D–A and A–DA′D–A structures and has promoted the rapid progress of OPVs.[8]

However, the asymmetric design is less applied to developing A_2–A_1–D–A_1–A_2 structured acceptors, though they have provided plentiful high-voltage OPVs with an open-circuit voltage (V_{OC}) around 1.0–1.3 V.[9,10] In addition, they are outstanding materials for application in indoor OPVs or ternary solar cells.[11,12] For example, a classic A_2–A_1–D–A_1–A_2 type NFA, **BTA3**, composed of an IDT core, a benzotriazole (BTA) bridge, and 2-(1,1-dicyanomethylene)rhodanine terminals, has shown a promising PCE of 10.5% with a V_{OC} of 1.24 V[13] in 2019. When **BTA3** is used as the third component, the corresponding ternary solar cells have attained over 18% efficiency.[14] Moreover, indoor OPVs based on different material combinations containing **BTA3** have produced high PCEs above 25%.[15,16] These great potentials drive us to conduct more profound research for constructing highly efficient BTA-based A_2–A_1–D–A_1–A_2 type acceptors.

Herein, we present an asymmetric A_2–A_1–D–A_1–A_2 structure acceptor, **HCl-BTA3**, by introducing chlorinated and non-halogenated BTA as the asymmetric A_1 units, respectively, as

[a] *CAS Key Laboratory of Nanosystem and Hierarchical Fabrication, CAS Center for Excellence in Nanoscience, National Center for Nanoscience and Technology, Beijing 100190, China. E-mail: tangal@nanoctr.cn, zhouej@nanoctr.cn*
[b] *Center of Materials Science and Optoelectronics Engineering, University of Chinese Academy of Sciences, Beijing 100049, China*
[c] *Henan Institutes of Advanced Technology, Zhengzhou University, Zhengzhou 450003, China*
[d] *Department of Chemical Science and Technology, Yunnan University, Kunming 650091, China*
[e] *College of Chemistry, Nanchang University, 999 Xuefu Avenue, Nanchang, 330031, China*

† Electronic supplementary information (ESI) available. See DOI: https://doi.org/10.1039/d2cc05631c

‡ These authors contributed equally to this work.

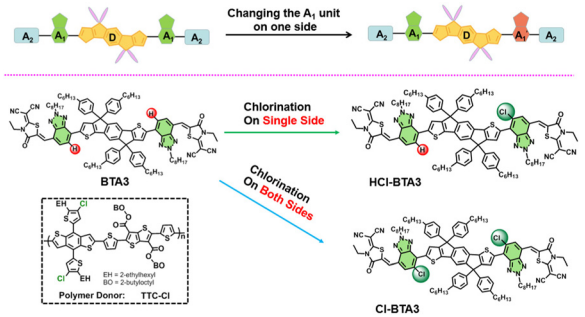

Fig. 1 The asymmetric molecular design strategies in A_2–A_1–D–A_1–A_2 small molecules and the chemical structures of **TTC-Cl**, **BTA3**, **HCl-BTA3**, and **Cl-BTA3** in this work.

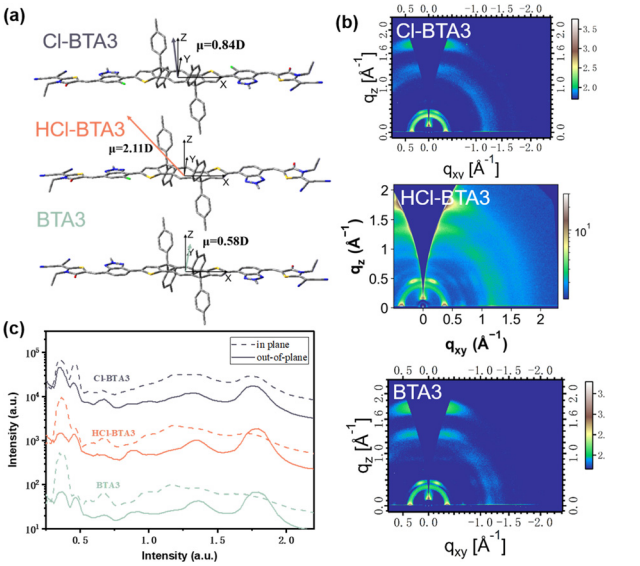

Fig. 2 (a) The optimized molecular conformation with dipole moments; (b) 2D-GIWAXS patterns of pure films; and (c) IP and OOP line cuts of the 2D GIWAXS patterns.

shown in Fig. 1. On the one hand, compared with symmetric **BTA3**, asymmetric **HCl-BTA3** exhibits a large molecular dipole moment and ordered molecular packing, contributing to the charge transfer and transport.[6,7] On the other hand, chlorination on a single side could provide a higher value of electroluminescence external quantum efficiency (EQE_{EL}) than chlorination on both sides,[17] generating a high V_{OC}. Here, we use a carboxylate-containing polymer, **TTC-Cl**, as the donor material because of its suitable energy levels and low energy disorder.[18] As a result, the **TTC-Cl**: **HCl-BTA3** blend attains a good balance between short-circuit current (J_{SC}) and V_{OC}, yielding a high V_{OC} of 1.20 V and a champion PCE of 11.2%. On the contrary, the **BTA3**-based device exhibits a high V_{OC} of 1.26 V but a low PCE of 9.67%, while the **Cl-BTA3**-based device yields a low V_{OC} of 1.15 V with a medium PCE of 11.05%. The results indicate that asymmetric chlorinated A_1 engineering is an effective strategy to modulate molecular energy levels, enhance molecular packing, decrease voltage loss, and thus improve photovoltaic performance.

HCl-BTA3 is synthesized by two steps of direct arylation coupling and then Knoevenagel condensation reaction, and the detailed synthesis procedures and characterizations are described in the ESI.† These three acceptor materials show good solubility in chloroform (CF), chlorobenzene (CB), and *o*-dichlorobenzene (*o*-DCB). As shown in Fig. S1 (ESI†), **HCl-BTA3** can maintain 95% weight at 365 °C and the corresponding temperatures for **BTA3** and **Cl-BTA3** are 395 °C and 339 °C,[19] respectively, indicating all three acceptors have good thermal stability.

We utilize density functional theory (DFT) calculations to explore the effect of asymmetric chlorination on molecular structures. As shown in Fig. 2a, an asymmetric design and strong electron-withdrawing Cl atoms afford **HCl-BTA3** a large molecular dipole moment of 2.11 Debye, whereas **BTA3** and **Cl-BTA3** with symmetric structures exhibit dipole moments of only 0.58 and 0.84 Debye, respectively. The larger dipole moments are thought to enhance the intermolecular interaction, improving the molecular packing and order. In addition, compared with **BTA3**, the introduction of Cl atoms distorts the conjugation backbone (Fig. S2, ESI†) because the large atomic radius of the Cl atom increases the dihedral angle between BTA and IDT units. Hence, chlorination may impede intermolecular packing to a certain extent.

We further conducted two-dimensional grazing incidence wide-angle X-ray scattering (2D-GIWAXS) to explore the effect of dipole moment changes on the molecular stacking of the neat film. As shown in Fig. 2b and c, all three neat films exhibit (100) and (200) diffraction peaks at a similar location with $q_{xy} \approx 0.36$ Å^{-1} and 0.67 Å^{-1} in the in-plane direction. However, the unilateral chlorinated **HCl-BTA3** and nonchlorinated **BTA3** exhibit a stronger (010) diffraction peak in the out-of-plane direction, indicating that both predominantly adopt a face-on orientation. The (010) diffraction peak of the bilateral chlorinated **Cl-BTA3** can be detected in both in-plane and out-of-plane directions, implying the coexistence of face-on and edge-on orientations. The π–π stacking distance of **HCl-BTA3** (3.50 Å) is smaller than that of **Cl-BTA3** (3.59 Å) and close to that of **BTA3** (3.50 Å). Although the chlorination may hinder the molecular packing, the extra intermolecular dipole–dipole interaction in **HCl-BTA3** can counteract this effect and form close molecular stacking.

The normalized absorption spectra of the four materials in the neat films are shown in Fig. 3a, and the data are summarized in Table S1 (ESI†). **HCl-BTA3** shows red-shifted absorptions of about 50 nm in the neat films compared to those in the CB solution, implying the existence of molecular aggregation. Compared with **BTA3** (λ_{max} = 654 nm), the maximum absorption peaks of **HCl-BTA3** and **Cl-BTA3** slightly red-shift, which may be related to the strong electron-accepting capability of the Cl atom. The optical bandgaps (E_g^{opt}) of **BTA3**, **HCl-BTA3**, and **Cl-BTA3** are 1.76, 1.72, and 1.72 eV, respectively, calculated from the absorption onsets of the films.

The frontier molecular orbital energy levels are tested by cyclic voltammetry. As shown in Fig. S3 (ESI†), the highest

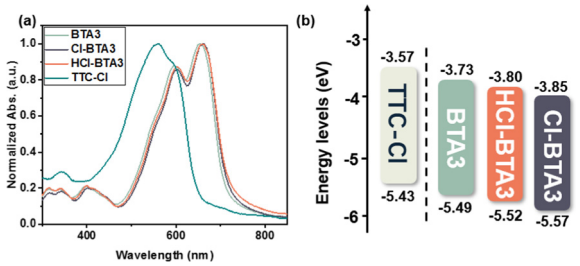

Fig. 3 (a) UV-vis absorption spectra in films of **TTC-Cl**, **BTA3**, **HCl-BTA3** and **Cl-BTA3**, and (b) the energy level diagram of the four compounds.

Table 1 Photovoltaic parameters of the optimal devices under the illumination of AM 1.5G, 100 mW cm^{-2}

Blends		V_{OC}	J_{SC} ($J_{calc.}$[b])		
Donor	Acceptor	(V)	(mA/cm^2)	FF	PCE
TTC-Cl	**BTA3**	1.26	11.30 (10.89)	0.679	9.67% (9.48 ± 0.15)[a]
	HCl-BTA3	1.20	13.42 (12.84)	0.696	11.20% (11.04 ± 0.11%)
	Cl-BTA3	1.15	13.81 (13.11)	0.696	11.05% (10.96 ± 0.09%)

[a] The values in parentheses are the average values with standard deviation obtained from 10 devices. [b] The values in parentheses are the integrated current density values calculated from EQE spectra.

occupied molecular orbital (HOMO) energy levels of **BTA3**, **HCl-BTA3**, and **Cl-BTA3** are calculated to be −5.49, −5.52, and −5.57 eV, respectively. The lowest unoccupied molecular orbital (LUMO) energy levels, deduced from the equation $E_{LUMO} = E_{HOMO} + E_g^{opt}$, are −3.73, −3.80, and −3.85 eV, respectively. The schematic energy-level diagrams of the four compounds are displayed in Fig. 3b. The density functional theory (DFT) calculations (Fig. S2, ESI†) revealed the same variation trend in the energy levels. With the gradual increase of Cl atoms on **BTA3**, the energy levels are reduced. The increased energy offsets between the donor and acceptor may further promote charge transfer.

To investigate the influence of asymmetric halogenated BTA on photovoltaic properties, we fabricated a traditional device structure of ITO/PEDOT:PSS/active layer/PFNBr/Al with a carboxylate-containing polymer, **TTC-Cl**, as the electron donor. The detailed optimization processes, including the weight ratio of the donor/acceptor (D/A), thermal annealing temperature, and solvent additive, are shown in Tables S2–S4 (ESI†). The current density–voltage (*J*–*V*) curves are displayed in Fig. 4a, and the detailed photovoltaic parameters are collected in Table 1. With the stepwise chlorination on BTA units, V_{OC} gradually declines from 1.26 V (**BTA3**) to 1.20 V (**HCl-BTA3**) and 1.15 V (**Cl-BTA3**). However, the J_{SC} of the corresponding devices exhibits opposite trends, increasing from 11.30 to 13.42 and 13.81 mA cm^{-2}, related to the efficient exciton dissociation and charge transport. The devices based on **TTC-Cl: HCl-BTA3** and **TTC-Cl: Cl-BTA3** show the same FF of 0.696, slightly higher than that of the **TTC-Cl: BTA3** (0.679) device. It is worth noting that the device based on **TTC-Cl: HCl-BTA3** exhibits the highest PCE of 11.20% due to the excellent balance between V_{OC} and J_{SC}, which is among the champion PCEs for high-V_{OC} carboxylate-containing polymer systems. The external quantum efficiency (EQE) curves in Fig. 4b indicate that all the devices show a similar photoresponse range of 300–750 nm, but the values of EQE_{max} gradually increase. The mismatch in J_{SC} between the value calculated from EQE curves and that measured from *J*–*V* curves is less than 5%.

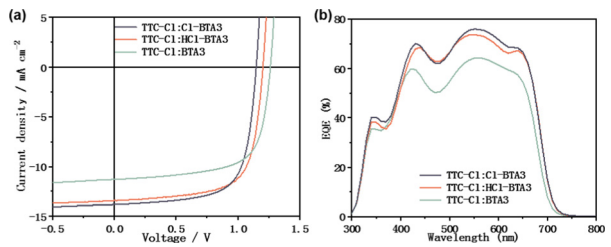

Fig. 4 (a) *J*–*V* curves of the optimized photovoltaic devices; (b) EQE spectra of the optimized solar cells.

We first perform photoluminescence (PL) quenching measurements to estimate the exciton dissociation efficiency in the hole transfer process with the excitation wavelength at 650 nm. Fig. S4 (ESI†) shows the calculated PL quenching efficiencies of 89.2%, 97.9%, and 98.8% for **TTC-Cl: BTA3**, **TTC-Cl: HCl-BTA3**, and **TTC-Cl: Cl-BTA3** blends, respectively, implying chlorination could promote the hole transfer. To explain these phenomena, we estimate the driving force for exciton dissociation in CT states. As shown in Fig. S5 (ESI†), the charge transfer energy (E_{CT}) can be deduced from the EL and highly sensitive Fourier-transform photocurrent EQE spectroscopy (FTPS). The E_{CT} of **TTC-Cl: HCl-BTA3** (1.70 eV) is lower than those of **TTC-Cl: BTA3** (1.73 eV) and **TTC-Cl: Cl-BTA3** (1.71 eV). Accordingly, the three devices exhibit a similar charge transfer driving force ($\Delta E_{CT} = E_g - E_{CT}$) around 0.1 eV. Hence, in the three systems of **TTC-Cl: BTA3**, **TTC-Cl: HCl-BTA3**, and **TTC-Cl: Cl-BTA3**, the different PL quenching efficiencies may be attributed to the molecular structure and molecular arrangement.

We further use atomic force microscopy (AFM) to investigate the influence of surface morphology on photocurrent, and the height images are shown in Fig. S6 (ESI†). The root-mean-square (RMS) roughness values of **TTC-Cl: BTA3**, **TTC-Cl: HCl-BTA3**, and **TTC-Cl: Cl-BTA3** blends are 1.33, 1.12, and 0.91 nm, respectively. As the degree of chlorination increases, the blend film has smoother surfaces due to the weaker crystallinity of **HCl-BTA3** and **Cl-BTA3**. The relatively rough surface of the **TTC-Cl: BTA3** film may exhibit a bulky domain size, also leading to a decrease in J_{SC} and FF. The GIWAXS data (Fig. S7, ESI†) reveal that, when blended with the donor, all three blend films show similar (100) diffraction peaks in the in-plane direction at q_{xy} = 0.33 $Å^{-1}$. The (010) diffraction peaks of the **BTA3**-, **HCl-BTA3**- and **Cl-BTA3**-based blend films are located at 1.75 $Å^{-1}$, 1.73 $Å^{-1}$, and 1.72 $Å^{-1}$, respectively, in the out-of-plane direction. The π–π stacking distances in the blend films are 3.59, 3.63, and 3.65 Å for the **TTC-Cl: BTA3**, **TTC-Cl: HCl-BTA3**, and **TTC-Cl: Cl-BTA3**, respectively, larger than that of their respective neat film. The smallest π–π stacking distance of the **BTA3**-based blend film demonstrates the strongest and

close molecular packing, consistent with the largest RMS value in AFM data.

The exciton dissociation probabilities (P_{diss}) were calculated from the J_{SC}/J_{sat} ratio (Fig. S8, ESI†), and the P_{diss} values for **BTA3**, **HCl-BTA3** and **Cl-BTA3** are calculated to be 94.9%, 95.2%, and 97.5%, respectively. Compared with the **TTC-Cl**: **BTA3**-based device, chlorination will improve the P_{diss} values. Furthermore, charge recombination was investigated by measuring the values of J_{SC} and V_{OC} at different light intensities (Fig. S9a and b, ESI†). According to the equation: $J_{SC} \propto P^{\alpha}$, the devices exhibit weak bimolecular recombination when α is close to 1. In our work, all the devices show similar bimolecular recombination (α = 0.97). The trap-assisted recombination was evaluated by the slope of the formula: $V_{OC} \propto nkT/q \ln(P)$. The slopes of **TTC-Cl**: **BTA3**, **TTC-Cl**: **HCl-BTA3**, and **TTC-Cl**: **Cl-BTA3** are 1.38, 1.25, and 1.23 kT/q, respectively, which indicate that chlorination is an effective strategy for reducing trap-assisted recombination. In addition, we used the space charge limited current (SCLC) method to measure the charge carrier mobility. As shown in Fig. S9c and d (ESI†), the values of hole mobility for **TTC-Cl**: **BTA3**, **TTC-Cl**: **HCl-BTA3**, and **TTC-Cl**: **Cl-BTA3** are 3.02×10^{-5}, 8.18×10^{-5}, and 9.02×10^{-5} $cm^2\ V^{-1}\ s^{-1}$, respectively. Moreover, the corresponding electron mobility values are 1.74×10^{-4}, 2.70×10^{-4}, and 3.81×10^{-4} $cm^2\ V^{-1}\ s^{-1}$, respectively. With chlorination on BTA units, **TTC-Cl**: **HCl-BTA3** and **TTC-Cl**: **Cl-BTA3** blend films exhibit increased and balanced carrier mobility, contributing to the improvement of J_{SC} and FF.

To get a deep insight into the high V_{OC} for these three blends, we further investigate the energy loss of these devices (Table S5 and Fig. S10a, ESI†). The radiative recombination voltage losses above the bandgap (ΔV_1) are around 0.286–0.287 V in the three devices. The radiative recombination voltage losses below the bandgap (ΔV_2) are 0.097, 0.093, and 0.095 eV for **TTC-Cl**: **BTA3**, **TTC-Cl**: **HCl-BTA3**, and **TTC-Cl**: **Cl-BTA3**, respectively. The somewhat smaller ΔV_2 for the asymmetric acceptor may be attributed to the minor energetic disorder with a smaller Urbach energy (E_u in Table S5, ESI†). ΔV_3 is the non-radiative recombination voltage loss and depends on EQE_{EL}. As shown in Fig. S10b (ESI†), the values of EQE_{EL} obviously decrease from **BTA3** through **HCl-BTA3** to **Cl-BTA3**, indicating that chlorination on the BTA unit will increase the non-radiative recombination voltage loss. As a result, the **TTC-Cl**: **BTA3** blend affords the smallest ΔV_3 of 0.18 V and **TTC-Cl**: **Cl-BTA3** yields the highest ΔV_3 of 0.27 V. The ΔV_3 of asymmetric **HCl-BTA3** falls between these two (0.23 V). Compared with symmetric **Cl-BTA3**, the decreased ΔV_3 and unchanged E_g afford **HCl-BTA3** a higher V_{OC} of 1.20 V.

In summary, we design a new asymmetric A_2–A_1–D–A_1–A_2 type acceptor, **HCl-BTA3**, by introducing a chlorine atom on one side of the A_1 unit. Compared with symmetric **BTA3**, asymmetric **HCl-BTA3** showed a larger dipole moment and stronger intermolecular arrangement, leading to efficient hole transfer and transport. Furthermore, compared with **Cl-BTA3**, unilateral chlorine substitution on BTA affords **HCl-BTA3** a higher value of EQE_{EL}, acting on the higher V_{OC}. As a result, the synergistic effect of the asymmetric structure and chlorination endows **HCl-BTA3** with a higher PCE of 11.2% with a V_{OC} of 1.20 V. Our work demonstrates that building an asymmetric A_2–A_1–D–A_1–A_2 structure is also an effective approach to construct efficient photovoltaic materials.

The authors acknowledge the support of the Strategic Priority Research Program of Chinese Academy of Sciences (Grant No. XDB36000000) and the National Natural Science Foundation of China (NSFC, No. 21875052, 51873044 and 52073067).

Conflicts of interest

There are no conflicts to declare.

Notes and references

1 J. Yuan, Y. Zhang, L. Zhou, G. Zhang, H.-L. Yip, T.-K. Lau, X. Lu, C. Zhu, H. Peng, P. A. Johnson, M. Leclerc, Y. Cao, J. Ulanski, Y. Li and Y. Zou, *Joule*, 2019, **3**, 1140–1151.
2 Y. Cui, Y. Xu, H. Yao, P. Bi, L. Hong, J. Zhang, Y. Zu, T. Zhang, J. Qin, J. Ren, Z. Chen, C. He, X. Hao, Z. Wei and J. Hou, *Adv. Mater.*, 2021, **33**, 2102420.
3 L. Zhu, M. Zhang, J. Xu, C. Li, J. Yan, G. Zhou, W. Zhong, T. Hao, J. Song, X. Xue, Z. Zhou, R. Zeng, H. Zhu, C. C. Chen, R. C. I. MacKenzie, Y. Zou, J. Nelson, Y. Zhang, Y. Sun and F. Liu, *Nat. Mater.*, 2022, **21**, 656–663.
4 C. He, Y. Pan, Y. Ouyang, Q. Shen, Y. Gao, K. Yan, J. Fang, Y. Chen, C.-Q. Ma, J. Min, C. Zhang, L. Zuo and H. Chen, *Energy Environ. Sci.*, 2022, **15**, 2537–2544.
5 K. Chong, X. Xu, H. Meng, J. Xue, L. Yu, W. Ma and Q. Peng, *Adv. Mater.*, 2022, **34**, 2109516.
6 W. Gao, M. Zhang, T. Liu, R. Ming, Q. An, K. Wu, D. Xie, Z. Luo, C. Zhong, F. Liu, F. Zhang, H. Yan and C. Yang, *Adv. Mater.*, 2018, **30**, 1800052.
7 M. Li, Y. Zhou, J. Zhang, J. Song and Z. Bo, *J. Mater. Chem. A*, 2019, **7**, 8889–8896.
8 Y. Zhang, Y. Ji, Y. Zhang, W. Zhang, H. Bai, M. Du, H. Wu, Q. Guo and E. Zhou, *Adv. Funct. Mater.*, 2022, **32**, 2205115.
9 B. Xiao, A. Tang, J. Zhang, A. Mahmood, Z. Wei and E. Zhou, *Adv. Energy Mater.*, 2017, **7**, 1602229.
10 A. Tang, B. Xiao, Y. Wang, F. Gao, K. Tajima, H. Bin, Z.-G. Zhang, Y. Li, Z. Wei and E. Zhou, *Adv. Funct. Mater.*, 2018, **28**, 1704507.
11 Y. Xu, Y. Cui, H. Yao, T. Zhang, J. Zhang, L. Ma, J. Wang, Z. Wei and J. Hou, *Adv. Mater.*, 2021, **33**, e2101090.
12 Z. Wang, A. Tang, H. Wang, Q. Guo, Q. Guo, X. Sun, Z. Xiao, L. Ding and E. Zhou, *Chem. Eng. J.*, 2023, **451**, 139080.
13 A. Tang, W. Song, B. Xiao, J. Guo, J. Min, Z. Ge, J. Zhang, Z. Wei and E. Zhou, *Chem. Mater.*, 2019, **31**, 3941–3947.
14 A. Lan, Y. Lv, J. Zhu, H. Lu, H. Do, Z.-K. Chen, J. Zhou, H. Wang, F. Chen and E. Zhou, *ACS Energy Lett.*, 2022, **7**, 2845–2855.
15 P. Bi, J. Ren, S. Zhang, J. Wang, Z. Chen, M. Gao, Y. Cui, T. Zhang, J. Qin, Z. Zheng, L. Ye, X. Hao and J. Hou, *Nano Energy*, 2022, **100**, 107463.
16 Z. Chen, T. Wang, Z. Wen, P. Lu, W. Qin, H. Yin and X.-T. Hao, *ACS Energy Lett.*, 2021, **6**, 3203–3211.
17 J. Qin, Z. Chen, P. Bi, Y. Yang, J. Zhang, Z. Huang, Z. Wei, C. An, H. Yao, X. Hao, T. Zhang, Y. Cui, L. Hong, C. Liu, Y. Zu, C. He and J. Hou, *Energy Environ. Sci.*, 2021, **14**, 5903–5910.
18 X. Li, A. Tang, Q. Guo, X. Guo, J. Chen, Q. Guo, M. Ji, Y. Meng, X. Li and E. Zhou, *ACS Appl. Mater. Interfaces*, 2022, **14**, 32308–32318.
19 T. Dai, Q. Nie, P. Lei, B. Zhang, J. Zhou, A. Tang, H. Wang, Q. Zeng and E. Zhou, *ACS Appl. Mater. Interfaces*, 2021, **13**, 58994–59005.

